Probing the surface of nanosheet H-ZSM-5 with FTIR spectroscopy

Probing the surface of nanosheet H-ZSM-5 with FTIR spectroscopy

B. T. L. Bleken, L. Mino, F. Giordanino, P. Beato, S. Svelle, K. P. Lillerud and S. Bordiga

Phys. Chem. Chem. Phys. (2013), 15, 32, 13363-13370

DOI: 10.1039/c3cp51280k

Probing the surface of nanosheet H-ZSM-5 with FTIR spectroscopy

Bjørn-Tore Lønstad Bleken,[a] Lorenzo Mino,[b] Filippo Giordanino,[b] Pablo Beato,[c] Stian Svelle[a], Karl-Petter Lillerud[a] and Silvia Bordiga*[a,b]

[a] *inGAP Centre of Research Based Innovation/Centre for Materials Science and Nanotechnology (SMN), University of Oslo, Department of Chemistry, N-0315 Oslo, Norway.*
[b] *Dipartimento di Chimica, NIS Centre of Excellence and INSTM Università di Torino, Via P. Giuria 7, 10125 Turin, Italy. silvia.bordiga@unito.it. tel: +390116708373*
[c] *Haldor Topsøe, Nymøllevej 55, DK-2800 Kgs. Lyngby, Denmark*

† Electronic Supplementary Information (ESI) available: FTIR spectra of H-ZSM-5 of conventional dimensions: Dehydrated and with H_2, CO and collidine adsorbed.

Herein we report FTIR *in-situ* adsorption of molecular hydrogen, carbon monoxide, water, methanol, pyridine and 2,4,6-trimethylpyridine (collidine) on nanosheet H-ZSM-5 recently made and studied in the methanol to hydrocarbons reaction (MTH).[1] The nature of the hydroxyl groups and surfaces species are described in detail. The IR spectrum of Nanosheet H-ZSM-5 is dominating by silanols, saturating the external surfaces. Acidity of Si(OH)Al is comparable to that observed in case of standard microcrystalline H-ZSM-5. The relevance of the external surface, allows recognizing Si(OH)Al species located at channel entrance and terminal Al-OH species, mostly all accessible to hindered molecules, such as collidine.

.

Introduction

Zeolites are microporous aluminosilicates used in various applications within ion-exchange, sorption processes and catalysis. The trivalent aluminium cations are present in tetrahedral positions in the same manner as silicon. Due to the four oxygen bonds aluminium induces a net negative charge to the framework which can be compensated by a proton. The proton is present on a hydroxyl bridge next to the aluminium and is a strong Brønsted acid site responsible for acid base catalysis within the material.

ZSM-5 is a zeolite of the MFI-framework and is responsible for a large fraction of catalysed petrochemical reactions for instance in the methanol-to-gasoline process.[2] The particle size of the crystallites varies in the µm range. ZSM-5 have two types of channels along the *a*- (zigzag channel) and *b*- (straight channel) crystallographic axis which intersects to form a three dimensional internal pore system. Microporosity imposes constraints to the size of the molecules able to enter inside the pores, moreover diffusion constrains of reagents and products can only be partially overcome by reducing the dimension of the crystallites.

In order to partially overcome these problems, that limits use of zeolites in some industrial applications, research has lately been focused on hierarchical zeolites in order to ensure fast diffusion in and out of the micropores via mesopores.[3] Carbon templating and post synthetic desilication are two pathways studied in order to achieve better diffusion.

Recently researchers in Ryoo's group have been able to synthesise ZSM-5 with sheet-like morphology, referred to as nanosheets, as an alternative to the two mentioned methods.[4,5] This is achieved by a tailored surfactant structure directing agent (SDA) which inhibits the growth of the crystallites along the *b*-axis of the framework. The growth along *a*- and *c*-axis then yields very thin sheets of the same magnitude as the *b* parameter of the MFI unit cell (~2 nm). This new unique crystal morphology drastically changes the ratio of internal and external surface. Considering a cubic MFI-crystal, 100 nm in each dimension, only ~2 % of the T-atoms are external T-atoms. A nanosheet crystallite with dimensions 16 × 4 × 19 nm is estimated to have ~20 % of the T-atoms on the external surface. The peculiar morphology of nanosheet ZSM-5, influences not only the abundance of silanols, but also affects the local structure of the Brønsted acid sites associated to the presence of framework Al^{3+}, as reported pictorially in Fig 1. Note that the picture is only a graphical representation and it is not exhaustive of all the possible structure that can be found.

The nanosheet ZSM-5 has been tested in a few catalytic applications such as conversion of "bulky" organic molecules[4,6,7] and in processes from the petrochemical industry. Choi et al.[4] showed that the nanosheet H-ZSM-5 was stable in the conversion of methanol to hydrocarbons.

Hu et al. tested nanosheet H-ZSM-5 with high Si/Al ratio (>200) in the methanol to propene process (MTP).[8] The nanosheet H-ZSM-5 was compared to a conventional H-ZSM-5 sample in the conversion of methanol at the same conditions. The nanosheet catalyst had 100 % conversion for 250 hours while the reference dropped from full conversion after 60 hours. The selectivity, at full conversion, to propene was 51 % in the nanosheet sample (*vs* 39 % in the reference sample) and it was also more selective to butylenes (22 % *vs* 19 %) while the selectivity to ethene (4.2 % *vs* 10.6 %) and aromatics (2.4 % *vs* 7.1 %) were lower. The authors found that the nanosheet H-ZSM-5 produced less coke and could accommodate more coke before deactivation compared to the conventional H-ZSM-5.

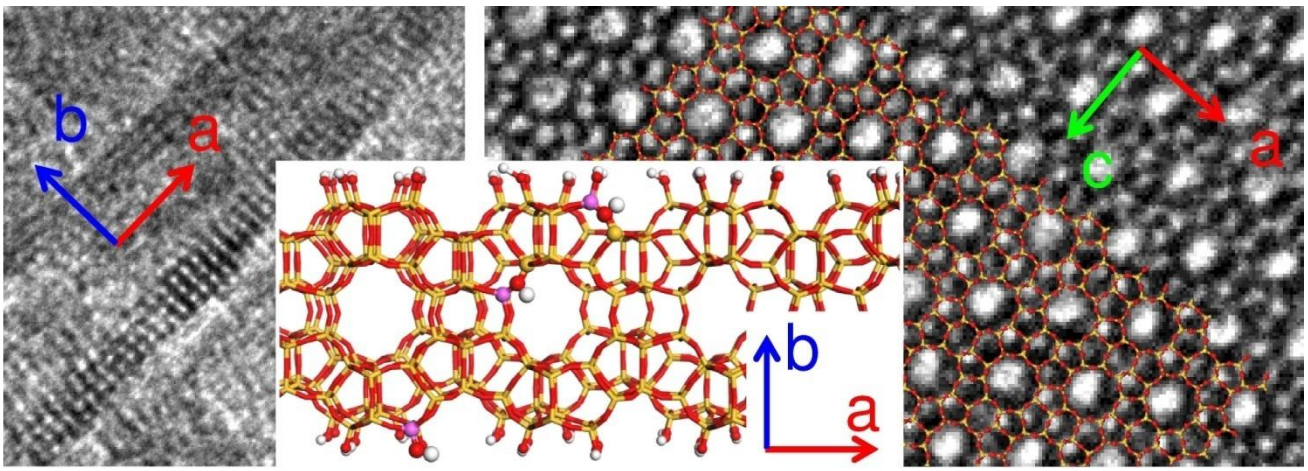

Fig. 1 HRTEM image of an H-ZSM-5 nanosheet seen from the side (left) showing a thickness of 4 nm. Top view HRTEM image (right) of a nanosheet with an MFI-framework overlay. A schematic illustration of a nanosheet and the relative position of Al in the framework are given in the middle. Three different Al environments are presented, although other possibilities may be plausible: A terminal AlOH (bottom), an internal classic Brønsted acid site Si(OH)Al (inside the channel) and an external less well defined Brønsted acid site where Al also has a terminal hydroxyl group (top). The external surface is otherwise covered with terminal SiOH groups.

Ethene conversion and heptane cracking were tested on nanosheet H-ZSM-5 and other nanosized H-ZSM-5 samples (particle size 0.13-13 μm).[9] The product selectivity for the different sized H-ZSM-5 samples was similar but the conversion after 1 h on stream of ethene over the nanosheets was about two orders of magnitude lower than for the catalyst with the smallest particle size. The same trend was found for the nanosheets in the heptane cracking: Similar product selectivity but lower conversion (~0.5) than the small particle catalyst. The authors concluded that the short residence time of reactants in the nanosheet microporous structure is responsible for the low conversion.

Similar findings was found by Verheyen et al who looked at *n*-decane isomerisation and hydrocracking over Pt/H-ZSM-5.[10] In this work they tested two nanosheet H-ZSM-5 samples of different thickness 2 and 8 nm in comparison with a reference H-ZSM-5. The isomerisation product distribution was similar in the three different catalysts. The two nanosheet samples did not show as clear selectivity to 2-, 3- or 4-methylnonane as was the case for the reference sample. Fast diffusion was pointed out as an explanation since 3- and 4-methylnonane diffuses slower in the MFI-framework they have a higher probability to react with another active site in the bulk reference sample than in the nanosheets to form the faster diffusing 2-methylnonane. At a reaction temperature of 438 K the thinnest nanosheet sample had a TOF half of the thicker nanosheet sample and the bulk reference. To reach full conversion the reaction temperature had to be raised 30 K higher for the thinnest nanosheets as compared to the thicker nanosheets and the reference.

We have recently shown that the selectivity in the MTH-reaction for nanosheet H-ZSM-5 is similar to a commercial H-ZSM-5 with the exception of low C_2 selectivity yielding very high C_3/C_2 ratios.[1] The same study indicated that the nanosheet sample was less active than the commercial H-ZSM-5. Based on the exceptional aspect ratio of the nanosheet crystallites and the lower activity we herein give a detailed description of the surface species on nanosheet H-ZSM-5 including the highly catalytic Brønsted acid sites.

Experimental procedure

Materials

The in-house nanosheet H-ZSM-5 samples were all synthesised as described in literature.[4,11] A gemini (diquarternary ammonium) surfactant was used as structure directing agent (SDA) on its bromide form. Its linear formula can be written as $CH_3(CH_2)_{21}$-$N^+(CH_3)_2$-$(CH_2)_6$-$N^+(CH_3)_2$-$(CH_2)_5CH_3$. Water glas and sodium aluminate were used as silicon and aluminium sources respectively. Sulphuric acid was added for lowering the pH. The overall chemical composition in the synthesis gel was 100 SiO_2 : 1 Al_2O_3 : 30 Na_2O : 24 H_2SO_4 : 7.5 SDA : 4000 H_2O. After calcination the zeolite was ion-exchanged with NH_4NO_3 following a subsequent calcination to obtain the H-form of the material. The nanosheet morphology was characterised by TEM and an extended Rietveld refinement relating powder XRD-peak broadening to physical dimensions. The material was further characterised by N_2-physisorption, NH_3-TPD, FTIR spectroscopy (without probe molecules), ^{27}Al and ^{29}Si MAS NMR and its performance in the MTH reaction.[1]

For this study additional elemental analysis was done on an Agilent 4100 MP-AES. 50 mg of zeolite was dissolved in 1 mL 15 wt% hydrofluoric acid for 30 minutes in a home made teflon container. The dissolved sample was introduced in a 50 mL polypropylene volumetric flask containing 0.15 g of boric acid used to neutralise any remaining hydrofluoric acid.

FTIR Spectroscopy

Water temperature programmed desorption

Water temperature programmed desorption was followed by using a commercial FTIR reactor-cell by *aabspec #2000-A* multi-mode, operating at atmospheric pressure in a wide range of temperature (up to 823 K) under flow conditions. The measurement was performed on pelletized sample (sieved fraction 140-200 mesh) under a flow of 5 mL/min of helium, by heating up at 5 K/min till 773 K. Infrared spectra were recorded

with a resolution of 4 cm^{-1} on a Perkin Elmer System 2000 spectrophotometer equipped with an MCT detector. Quantitative water desorption was followed by integrating the δ(OH) signal at 1620 cm^{-1}: Curve fitting analysis was performed with the Levenberg-Maquardt method by using the OPUS software (Bruker Optik). Mixed Gauss-Lorentzian functions were used.

FTIR of adsorbed probe molecules

For FTIR spectroscopy with probe molecules all samples were pressed into self-supporting wafers and measured in transmission mode in FTIR instruments equipped with MCT-detectors having a resolution of 2 cm^{-1} unless otherwise noted.

The wafers were pre-treated in vacuum at 823 K for 4 hours before recording the background spectrum. 40 mbar of H_2 were introduced into the cell while cooling down to 15 K allowing the H_2 to adsorb. Consecutively after evacuating H_2, the sample was heated to 60 K and 40 mbar of CO were dosed. H_2 and CO sorption were measured on a Bruker Equinox 55 with a resolution of 1 cm^{-1} equipped with a cryostat in a homemade assembly.[12] Methanol, ethylene, pyridine and 2,4,6-trimethylpyridine (collidine) were adsorbed at room temperature.

Results and discussion

The effect of thermal activation in flux on the infrared spectra of nanosheets ZSM-5 is illustrated in Fig. 2a (ν(OH)-region). At 300 K, the IR spectrum of nanosheet ZSM-5 is characterized by a broad signal centred at 3400 cm^{-1}. Along the thermal treatment, apart from a continuous decrease in intensity of the main band, we observe a progressive blue shift of its maximum, testifying the removal of H-bonded water molecules and of H-bonded silanols chains, with the parallel growth of the band at 3736 cm^{-1}. A semi-quantitative analysis of water removal is reported in Fig. 2b, that shows the amount of water, as calculated from the integrated area of the band at 1620 cm^{-1} (bending mode of water). From the graph it is clear that at 473 K, molecular water has been removed. Above this temperature, the broad and intense absorption observed in the IR spectrum (maximum at 3500 cm^{-1}) is more likely associated to H-bonded hydroxyls than to water. Slowly this band evolves reducing in intensity in favour of the band at 3736 cm^{-1}. The final spectrum (bold black curve) is characterised by a maximum at 3736 cm^{-1} with a broad tail extending to 3200 cm^{-1} and a component at 3612 cm^{-1} ascribable to strong Brønsted acid sites. Generally speaking, isolated external silanols are expected at 3745 cm^{-1} so, the fact that the final spectrum shows a complex band where the maximum appears at 3736 cm^{-1}, implies the presence of abundant defective species still engaged in week H-bonds at the external surfaces and at the pore mouth. The broad adsorption extending till 3200 cm^{-1} is associated to medium and long chains of H-bonded silanols present inside the pores (internal nests). Part c of Fig.1 reports in the full length of the medium infrared spectrum, the dehydrated sample activated in vacuum. In vacuum the extension of dehydroxylation is higher as the silanol band is sharper than what observed upon activation in helium flux. In this case the maximum is observed at 3745 cm^{-1} testifying that the abundance of free silanols has increased. In the meantime the broad band associated to H-bonded silanols mostly located inside the pores, has drastically reduced and only a tail at the bottom of the main peak at 3745 cm^{-1} is observed. Vacuum activation force silanol condensation and the consequent formation of strained Si-O-Si bridges which are characterised by bands in the region 950-850 cm^{-1}.[13,14] In this specific case a strong component is clearly visible at 895 cm^{-1}, while in other samples its presence is less evident. See for example the data reported in ESI Fig. S1, that compare a different nanosheet ZSM-5 with two commercial samples. Generally speaking the intensity of this bands and the temperature at which it is observed is an indication of the number of defects present in the material.[13,14]

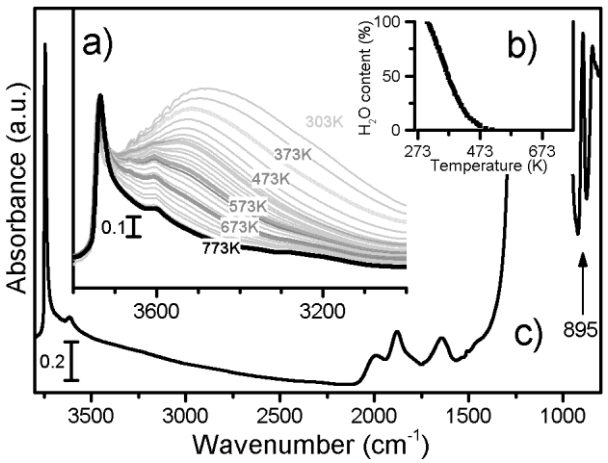

Fig. 2 a) ν(OH) stretching modes evolution upon water temperature programmed desorption in helium flow, b) the relative water content as a function of temperature and c) dehydrated nanosheet H-ZSM-5 activated in vacuum at 823 K.

Interaction with H_2

As previously described[15], generally hydrogen is dosed at room temeperature and the progressive cooling of the sample is monitored by subsequent acquisitions (see the spectra sequence in Fig. S2). The temperature decrease (from 250 to 100 K) causes a slight blue shift of the silanol peak (band I) and apparance of two new bands non distinguishable at room temperature. The first at 3736 cm^{-1} (vide supra) and the second at 3670 cm^{-1}, previously assigned to (partially) extra framework aluminium (AlOH)[16], or associated to Al species present on the external surfaces of microcrystals (band II). These species have been recently discussed in the case of amorphous silica-alumina.[17-20] Hydroxyl groups associated to Si(OH)Al sites (band III) undergo an upward shifts of 12 cm^{-1} upon cooling. In the temperature range between 100 to 60 K, we observe a progressive shift of the maximum at 3670 cm^{-1} to 3665 cm^{-1}, while the band associated to the strong Brønsted sites is totally eroded and the parallel growth of a band at 3572 cm^{-1} is observed.

In the temperature range 60-15 K, the component at 3670 further shifts to 3655 cm^{-1} and a tail on the low frequency side, suggesting the probable presence of a component at 3639 cm^{-1}, appears. This observation suggests that the species associate to the band II are hetrogeneous and that their acidity is intermediate between SiOH (band I) and Si(OH)Al (band III). At 15 K, most of the silanols are perturbed giving rise to a band centered at 3731 cm^{-1}. The H_2 stretching frequency counterpart (see the inset of Figure S2) confirms that: i) in the range 250-100 K hydrogen is not perturbed through any specific iteraction, ii) between 100 to 60 K hydrogen forms first adducts with strong Brønsted sites and

then with the less acidic species (vide supra), iii) furter temperature decrease changes the entire profile of the spectra, finally dominated by physisorbed hydrogen. Fig. 3 shows IR spectra evolution upon hydrogen desorption at 15 K. Left panel shows the ν(OH) region and the right panel shows the ν(HH) region. Lower curves in both panels are related to low coverage of H_2 adsorped on the sample in which the probe is mostly interacting with strong Brønsted sites: Si(OH)Al. The top set of curves are related to higher coverage of H_2 where hydrogen is interacting with the majority of hydroxyles. In the ν(OH) region a segment of data for each set have been magnified for better readability. The bold grey curve is the dehydrated sample after removal of H_2, the thin black curves in both sets represent the same spectrum and the bold black curve is the maximum coverage of H_2.

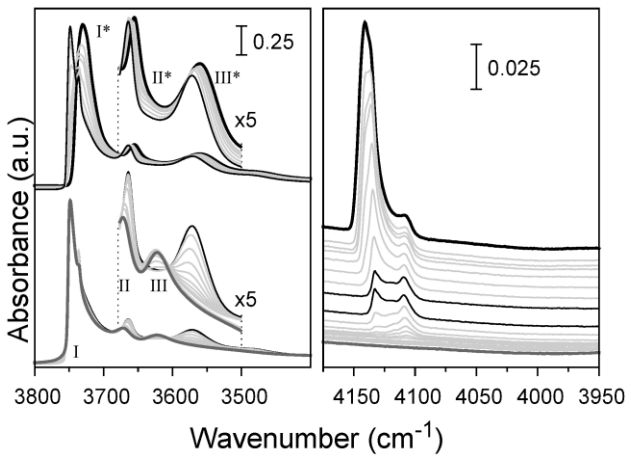

Fig. 3 H_2 desorption at 15 K with emphasis on the ν(OH) region (left panel) and the ν(HH) region (right panel). Upper set of curves relate to high coverage of H_2 and the bottom set is related to lower coverage of H_2. Segments of data for both sets have been magnified in the left panel.

At maximum H_2 loading the spectrum is dominated by the very intense band (I*) at 3731 cm^{-1} by a minor component (II*) at 3655 cm^{-1} (with a tail that could imply a component centered around 3639 cm^{-1}) and by the component at 3560 cm^{-1} (III*). The progressive decrease of the hydrogen equilibrium pressure implies the partial restoration of all the silanol, a change in the specta profile around 3639 cm^{-1}, accompanied by a blue shift of the maximum associated to band II* that moves back from 3655 cm^{-1} to 3665 cm^{-1}, the shift of the maximum from 3560 to 3570 cm^{-1}. All these changes suggest an evolution in the hydrogen packing inside the zeolites cages and the disruption of the weaker interactions. The set of curves associated to the effect of further decreases in the hydrogen equilibrium pressure are reported in the bottom part of Fig. 3. Most relevant changes are shown in the inset, where it is illustrated the progressive restoration of the unperturbed Si(OH)Al species (band III, maximum at 3624 cm^{-1}) and the evolution of the maximum of band II at 3665 cm^{-1} to the weaker maximum centered at 3670 cm^{-1}. The shift of the Si(OH)Al sites ($\Delta\nu$= -52 cm^{-1}) is accordance with previous work[16]

In the ν(HH) region, from low to high hydrogen coverages, the following signals are observed: i) the first ν(HH) band, seen at 4109 cm^{-1}, is due to molecular hydrogen interacting with Si(OH)Al. The increase in intensity is in accordance with the corresponding Si(OH)Al shift observed in the ν(OH) region. A second signal in the ν(HH) region appears at 4133 cm^{-1} related to the SiOH-H_2 adduct. No clear evidence of a specific component ascrivable to the formation of AlOH-H_2 adducts is observed. We only note a illdefined absorption centered at 4120 cm^{-1} that progressively grow mixing wih the contribution due to physisorbed hydrogen.

At higher loadings the signal, due to SiOH-H_2 interactions, moves to 4136 cm^{-1} where it becomes a shoulder of a new and more intense band at 4140 cm^{-1}. The broad character of the band suggests that H_2 is not entrapped inside small cavities as observed before in other microporous materials such as Silicalite,[15] H-SSZ-13 and SAPO-34.[21] No signal is seen around 4020 cm^{-1} previously reported to be hydrogen in interaction with Al^{3+} (Lewis acid site).[16] For sake of comparison data obtained on a commercial microcrystalline H-ZSM-5 (Si/Al= 40) are reported in ESI, in Fig. S3.

Interaction with CO

Fig. 4 shows CO desorption at 60 K, performed after complete desorption of hydrogen. The left panel shows the ν(OH) region, the top right panel shows the ν(CO) region at all degrees of coverage while the bottom right panel shows only the ν(CO) region of spectra at the lowest coverage of CO. Upper curves are related to high loading of CO and the bottom curves are related to low loading of CO. The bold grey curve is the sample after complete removal of H_2, the bold black curve is the highest loading of CO and the thin black curves in both sets represent the same spectrum.

At lower coverage of CO, the shift of the Si(OH)Al band is clearly seen by the decreasing band at 3620 cm^{-1} and the increasing band at 3300 cm^{-1}. The signal at 3670 cm^{-1} (associated to the presence of Al, most probably at the external surfaces) is nearly left unchanged, while the SiOH-shoulder, at 60 K observed at 3731 cm^{-1}, increases in intensity. The main SiOH band does not change.

At higher coverage of CO, the SiOH band including the shoulder at 3731 cm^{-1} decreases and a new band, caused by the SiOH-CO adduct, grows at 3655 cm^{-1}. This new maximum shows a very broad tail in the low frequency side that can be interpreted as a result of a very pronounced heterogeneity of sites. Note that even at maximum coverage not all the silanols are affected by CO, being a portion at higher frequency, left unperturbed.

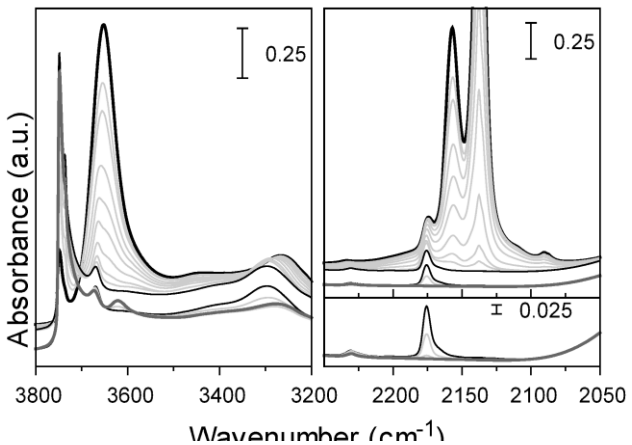

Fig. 4 CO desorption with emphasis on the ν(OH) region (left panel) and ν(CO) region (right panel). Upper set of curves relate to high coverage of CO and the bottom set is related to lower coverage of CO. A segment of data for the bottom set has been magnified in the right panel.

The appearance of an intense band superimposing the component at 3670 cm^{-1}, does not allow any description of its fate upon CO dosages. It is possible that its erosion contributes to the formation of the broad tail of the band centred at 3655 cm^{-1} and/or it could be associated with the appearance of the component at 3440 cm^{-1}, In respect to this last assignement we mention that recently similar features were described in terms of resonance effects[22]. At this stage we cannot make a final assignment. At maximum CO coverage, the formation of condensed CO phase gives rise to an additional downward shift of the band from 3300 cm^{-1} to 3267 cm^{-1}.

The corresponding interactions are seen in the ν(CO) region (Fig. 4 right panel). CO interaction with Si(OH)Al is seen at 2175 cm^{-1}. Note that the band is asymmetric on the high frequency side, suggesting the presence of heterogeneity of sites. A possible explanation is that this tail is due to the adducts formed with OH groups associated to framework Al sites on the external surfaces. In this respect, it is interesting to mention the recent work made on amorphous silica-alumina combining both experiments and theory.[20] At the lowest coverage a CO stretch related to Al^{3+} (Lewis acid sites) is present at 2230 cm^{-1} although very weak. At higher coverage the 2175 cm^{-1} signal remains rather constant. Two new signals appear simultaneously at 2158 cm^{-1} due to CO adsorbed on various SiOH species which probably are of similar acidity and 2138 cm^{-1} assigned to condensed liquid like CO in the pores of the zeolite. A shoulder of the previous signal at 2110 cm^{-1} can be observed at the highest loading as well as a new band at 2090 cm^{-1}. Temperature-dependent IR studies have attributed these kind of weak bands, which are red-shifted with respect to gas phase, to the formation of less stable adducts in which CO is interacting through the oxygen end.[23] However a contribution to these spectral features from the natural fraction of the $^{13}C^{16}O$ isotope (about 1%) cannot be excluded.[24]

For sake of comparison data obtained on a commercial microcrystalline ZSM-5 (Si/Al= 40) are reported in ESI, in Fig. S4. Also in this case, major differences observed in case of H-ZSM-5 nano sheets are: i) enhanced intensities of silanols, ii) low intensity and asymmetry of the band due to strong Brønsted sites.

Interaction with methanol and ethylene

The reactivity of the material was tested following the interaction with methanol and ethylene. The results are reported in Fig. 5 and 6 respectively. Adsorption of methanol in acidic zeolites has been studied extensively as it is the reagent of the well-known MTH process. As proton affinity of methanol is significantly greater than those of the already discussed probes, in this case we expect significant changes in the FTIR spectra.

The bold dark grey curve in Fig. 5 represents the dehydrated sample before adsorption of methanol. Methanol loading causes a progressive decrease of the SiOH main band continuing to total erosion. The Si(OH)Al band at 3612 cm^{-1} readily disappears. In parallel the methanol is responsible for a growth of a broad component with a maximum at 3375 cm^{-1}. This signal is assigned to both hydrogen bonding between methanol molecules and hydrogen bonding between methanol and silanol groups. A second maximum is found at 3623 cm^{-1} due to the chain formation by hydrogen bonding between several methanol molecules.[25] ν(CH) in the methanol is slightly moving to lower frequency with increased coverage: (i) $\nu_{asym}(CH_3)$ is present at 2998 and 2959 cm^{-1} at low coverage moving to 2985 and 2950 cm^{-1} at maximum coverage, (ii) the $\nu_{sym}(CH_3)$ moves from 2858 cm^{-1} to 2842 cm^{-1}.

On increasing coverage of methanol the scattering profile becomes more pronounced with an increase of the absorption values on the low frequency side of the spectrum (3000-700 cm^{-1} range). This phenomenon has been already observed and is due to the appearance of a very broad absorption due to strong H-bonding species formed between CH_3OH and Si(OH)Al.[25] At the maximum coverage the rotovibrational contribution of methanol is seen at 3680 cm^{-1}. The spectra of adsorbed methanol does resemble more the aluminium free Silicalite-1 than a ZSM-5.[26] This sample has one major component related to SiOH interactions as already discussed. Two more major absorptions have been reported for H-ZSM-5 around 2400 and 1650 cm^{-1} characterised by strong hydrogen bonding with the additional protonation of the methanol.[25]

First dosage of methanol erodes the band at 895 cm^{-1} (Fig. 5 inset), suggesting that it is due to strained Si-O-Si bridges present in the highly dehydroxylated sample. The methanol probably breaks the bridges in favour for the formation of a SiOH and $SiOCH_3$. The spectrum collected after evacuation at room temperature (bold light grey curve), testifies that methanol is not completely reversible at room temperature. The silanol band is not completely restored and a broad background is still present.

To verify the Brønsted acidity ethylene was let into the cell containing a dehydrated sample. The thin grey curve in Fig. 6 is the spectrum recorded right after addition of ethylene. The gas phase ethylene can be seen by the ν(CH) at 2889 cm^{-1} and δ(CH) at 1444 cm^{-1} which is shifted to 1440 cm^{-1} in the adsorbed state.[27]

Upon mild heat treatment formation of polyethylene takes place and after desorption of excess ethylene (bold black curve) the irreversible process is visible. The Si(OH)Al sites are not restored. The SiOH band is not directly affected in the polymerisation, but has a longer tail as the polymer chains engage some SiOH in weak interactions. Saturated methyl and methylene groups are present by $\nu(CH_3)$ at 2956 and 2876 cm^{-1} and $\nu(CH_2)$ at 2936 and 2862 cm^{-1}. Two δ(CH) in the saturated hydrocarbon

chain are also seen at 1469 and 1459 cm^{-1}. From the inset in Fig. 6 it is noted that the band at 895 cm^{-1} is not affected by ethylene, confirming the previous assignment given to strained Si-O-Si bridges. The sharp band at 950 cm^{-1} is due to gas phase ethylene (CH_2 wag b_1u).[28]

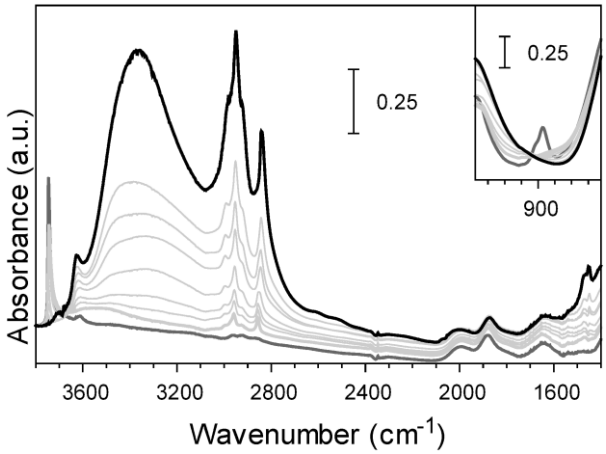

Fig. 5 Methanol sorption from dehydrated nanosheet H-ZSM-5. Maximum coverage of methanol at the top (black curve) and decreasing coverage (grey curves). The spectrum of the dehydrated sample (bold grey) is placed at the bottom as reference. The 895 cm^{-1} band is presented in the inset.

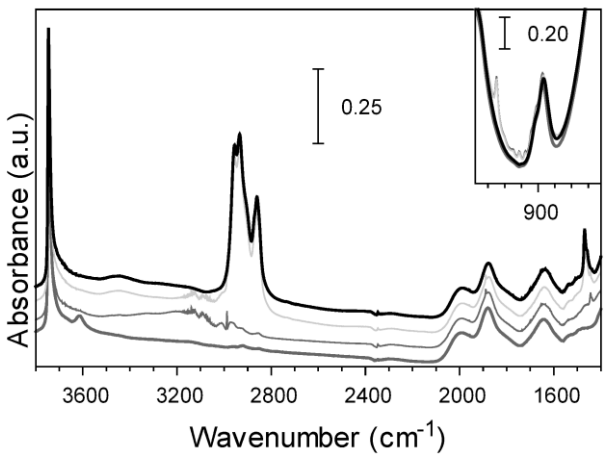

Fig. 6 Dehydrated nanosheet H-ZSM-5 (bottom bold grey curve), contacted with ethylene at room temperature (grey curve), after polymerisation at 373 K (light grey curve), and after evacuation at room temperature (top black). The spectra are shifted on the y axis for clarity. The 895 cm^{-1} band is presented in the inset.

Interaction with pyridine and collidine

In order to explore the accessibility of the protons, two additional probes were used. Fig. 7a and b shows the FTIR spectra after adsorption of pyridine and collidine respectively. The two molecules are characterised by a proton affinity high enough to deprotonate the Brønsted acid sites but they are quite different in dimension, as collidine is too large to enter the pores in H-ZSM-5. Part a) in Fig. 7 are spectra from the pyridine adsorption showing the ν(OH) region (left) and the ring modes region (inset). Part b) in Fig. 7 displays spectra from the collidine adsorption. Dark grey curves are the dehydrated sample, light grey curves are with the probe loaded and black curves are after evacuation at room temperature. Wavenumbers from literature[29,30] are highlighted by an asterisk (*) which represents probe molecules which are physisorbed or hydrogen bonded to the surface and a vertical bar (|) which represents protonated probe molecules.

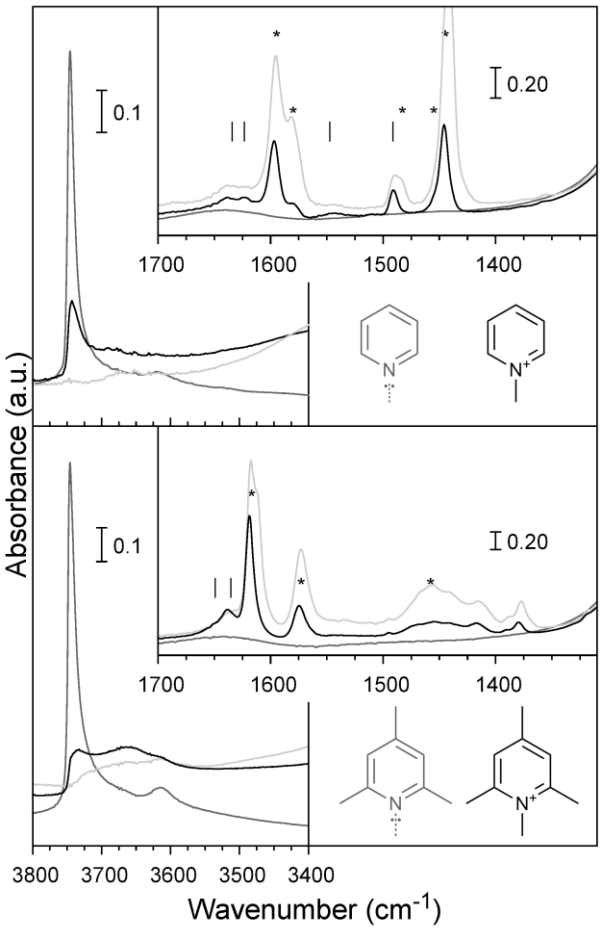

Fig. 7 FTIR spectra of adsorption of pyridine (top) and collidine (bottom) on the dehydrated sample. The ν(OH) region is presented to the left and the ring mode vibrations of the probes in the insets. Dark grey curves are before adsorption, light grey curves are after adsorption of the probe and black curves are after evacuation of the probe at room temperature. * refers to ring modes of physisorbed or hydrogen bonded probes. | refers to ring modes of the probes protonated by the Brønsted acid sites.

In case of pyridine adsorption, both Si(OH)Al and SiOH are completely eroded. (light grey curve), while for collidine a residual fraction of unreacted hydroxyls is observed: ill-defined absorption centred at 3690 cm^{-1} and a week residual band at 3612 cm^{-1}. As the size of collidine (7.4 Å) is too large to enter the 10-rings (5.1×5.5 and 5.3×5.6 Å) of ZSM-5, this indicates that most of the strong Brønsted sites are located close to the surface where collidine can access them, moreover, the persistence of a component at 3690 cm^{-1}confirms the fact that at least a fraction of H-bonded silanols are located inside the pores, being not accessible to collidine. After evacuation at room temperature (black curves) some of the SiOH signal is recovered (maximum at 3735 cm^{-1}. We observe that most of the free SiOH are still holding on to the probes at this point, while the bands at 3690 cm^{-}

and at the residual component at 3612 cm^{-1} are nearly unchanged, as expected by species that were not involved by collidine interaction. The highlighted ring modes, presented in the insets of Fig. 7a (pyridine) and 7b (collidine), are sensitive to the nature of the surface where the probe is adsorbed. The presence of protonated pyridine is seen by four signals (|) related to the ring modes of pyridinium (1634 cm^{-1} 8a, 1623 cm^{-1} 8b, 1491 cm^{-1} 19a and 1547 cm^{-1} 19b).[29] The collidinium cation has its 8a and 8b ring mode vibration at 1635 and 1649 cm^{-1} respectively.[30] Clear and stable signals are present at these wavenumbers even after evacuation. This allows us to conclude that there must be Si(OH)Al sites at the external surface and/ or in the vicinity of the pore mouths.[30]

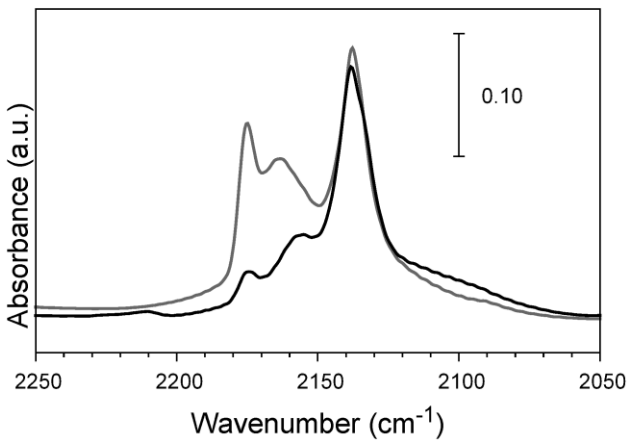

Fig. 8 FTIR difference spectra of CO adsorption at 77 K on dehydrated H-ZSM-5 nanosheets (grey) and dehydrated H-ZSM-5 nanosheets saturated with collidine (black).

Consecutive adsorption of collidine and CO was performed to discriminate the fraction of sites not accessible to collidine but available to interact with a probe that can easily go inside the channels. A comparison of FTIR difference spectra of CO adsorbed on a dehydrated sample and a sample where collidine was pre-adsorbed is shown in Fig. 8 (physisorbed collidine was removed through a long degassing at RT). The amounts of SiOH and Si(OH)Al sites probed by CO, are clearly substantially reduced when collidine is adsorbed on the sample (black curve). Nevertheless, the presence of the ν(CO) vibrations at 2175 and 2158 cm^{-1} in the collidine saturated sample indicates that a small fraction of sites are unavailable for collidine, as expected in case of a standard H-ZSM-5 (see for sake of comparison the data is reported in Fig S5 in ESI). However, the fact that nanosheets H-ZSM-5 crystals maintain intact shape selectivity in the MTH reaction,[1] suggests that part of the sites protonated by collidine are located inside the channels but in close proximity to the channels mouth.

Conclusions

IR spectroscopy performed in controlled atmosphere and with the help of probe molecules allowed to reveal characteristics of surface species present in nanosheet H-ZSM-5.

Water desorption from the sample is easier than in a standard zeolite. This behaviour is also related to the crystals morphology (nanosheets) that allows an easier diffusion of water out of the particles. Upon water removal and hydroxyl condensation, abundant strained Si-O-Si bridges are present, testified by a strong IR signal at 895 cm^{-1}. This band, associated to structural defects was unaffected by H_2, CO and ethylene (Lewis bases) while methanol interacts instantaneously with these sites.

The unique morphology of the MFI zeolite shows a characteristic distribution of hydroxyl groups. Silanols are responsible for the most pronounced absorption in the ν(OH) region due to the unsaturated SiO_2 network at the external surface.

IR spectra collected at low temperature show a peculiar component in the ν(OH) region (3670 cm^{-1}). A possible assignment, that however is not conclusive, is that it could be ascribed to framework Al sites present in the external surfaces as AlOH. At the present stage, as the number of systems investigated is relatively small, we do not have a confirmation of this assignment. The low ratio of external surface area over bulk volume for a microcrystalline zeolite decreases the abundance of these eventual AlOH species below IR sensitivity. (Figs S3 and S4 bold black curves, obtained at low temperature and in absence of probes). The fraction of framework aluminium associated to this band gives rise to a family of sites characterized by a slightly lower acidity in respect to the traditional Si(OH)Al internal site, as detected by low medium strength probes (H_2, CO, CH_3OH). Conversely pyridine and collidine protonates the majority of Al compensating charges.

H_2 and CO adsorption probed the acidity of nanosheet H-ZSM-5. The shift of the Si(OH)Al signal by adsorption of H2 and CO was in full agreement with what obtained in case of standard zeolites. ($\Delta\tilde{\nu}$ = -52 and -320 cm^{-1} in case of H_2 and CO respectively).

IR spectra of methanol adsorption was dominated by the features characteristic for aluminium free zeolites, nevertheless the presence of some strong Brønsted acid sites was recognized by the appearance of a very broad background extending in the full MID range. Moreover, when the sample was contacted with ethylene and mildly heated, it polymerised into polyethylene, thus testifying the reactivity of the nanosheet H-ZSM-5.

The acid site accessibility was determined by the use of pyridine and collidine. After degassing at room temperature both pyridinium and collidinium were observed by IR. As already discussed above it seems like all Brønsted acid sites are available for collidine as the Si(OH)Al is undetectable after adsorption. For a microcrystalline H-ZSM-5 sample the situation was very different, as after adsorption of collidine, the change in the Si(OH)Al is hardly detectable as compared to the spectrum of the dehydrated microcrystalline H-ZSM-5.

From collidine adsorption and consecutive adsorption of collidine and CO we conclude that a substantial amount of the strong Brønsted acid sites are located inside the channels but in close proximity to the channels mouth.

The lower concentration of strong Brønsted acid sites Si(OH)Al inside the confined reaction volume of the zeolite pore could be the cause for the observed lower activity of nanosheet H-ZSM-5 as compared to conventional H-ZSM-5.

Acknowledgements:
BTLB is grateful for a scholarship from the Research Council of Norway through RENERGI (Project No. 182532/I30). This publication is part of the inGAP Centre of Research Based Innovation, which receives financial support from the Research Council of Norway under Contract No. 174893 and of Progetto di Ateneo dell'Università di Torino 2011-1A line Contract No. ORTO11RRT5**.**

References

1. B.-T. L. Bleken, D. S. Wragg, B. Arstad, A. E. Gunnæs, J. Mouzon, S. Helveg, L. F. Lundegaard, P. Beato, S. Bordiga, U. Olsbye, S. Svelle and K. P. Lillerud, *Top. Catal.*, 2013, 10.1007/s11244-013-0010-9, 1-9.
2. U. Olsbye, S. Svelle, M. Bjørgen, P. Beato, T. V. W. Janssens, F. Joensen, S. Bordiga and K. P. Lillerud, *Angew. Chem., Int. Ed.*, 2012, **51**, 5810-5831.
3. J. Perez-Ramirez, C. H. Christensen, K. Egeblad, C. H. Christensen and J. C. Groen, *Chem. Soc. Rev.*, 2008, **37**, 2530-2542.
4. M. Choi, K. Na, J. Kim, Y. Sakamoto, O. Terasaki and R. Ryoo, *Nature*, 2009, **461**, 246-249.
5. K. Na, M. Choi, W. Park, Y. Sakamoto, O. Terasaki and R. Ryoo, *J. Am. Chem. Soc.*, 2010, **132**, 4169-4177.
6. J. Kim, W. Park and R. Ryoo, *ACS Catal.*, 2011, **1**, 337-341.
7. K. Na, C. Jo, J. Kim, K. Cho, J. Jung, Y. Seo, R. J. Messinger, B. F. Chmelka and R. Ryoo, *Science*, 2011, **333**, 328-332.
8. S. Hu, J. Shan, Q. Zhang, Y. Wang, Y. Liu, Y. Gong, Z. Wu and T. Dou, *Appl. Catal., A*, 2012, **445–446**, 215-220.
9. J. K. Reddy, K. Motokura, T.-r. Koyama, A. Miyaji and T. Baba, *J. Catal.*, 2012, **289**, 53-61.
10. E. Verheyen, C. Jo, M. Kurttepeli, G. Vanbutsele, E. Gobechiya, T. I. Korányi, S. Bals, G. Van Tendeloo, R. Ryoo, C. E. A. Kirschhock and J. A. Martens, *J. Catal.*, 2013, **300**, 70-80.
11. K. Na, W. Park, Y. Seo and R. Ryoo, *Chem. Mater.*, 2011, **23**, 1273-1279.
12. G. Spoto, E. N. Gribov, G. Ricchiardi, A. Damin, D. Scarano, S. Bordiga, C. Lamberti and A. Zecchina, *Prog. Surf. Sci.*, 2004, **76**, 71-146.
13. Y. Inaki, H. Yoshida, T. Yoshida and T. Hattori, *J. Phys. Chem. B*, 2002, **106**, 9098-9106.
14. A. Zecchina, S. Bordiga, G. Spoto, L. Marchese, G. Petrini, G. Leofanti and M. Padovan, *J. Phys. Chem.*, 1992, **96**, 4991-4997.
15. C. Lamberti, A. Zecchina, E. Groppo and S. Bordiga, *Chem. Soc. Rev.*, 2010, **39**, 4951-5001.
16. A. Zecchina, G. Spoto and S. Bordiga, *Phys. Chem. Chem. Phys.*, 2005, **7**, 1627-1642.
17. C. Chizallet and P. Raybaud, *Angew. Chem., Int. Ed.*, 2009, **48**, 2891-2893.
18. C. Chizallet and P. Raybaud, *ChemPhysChem*, 2010, **11**, 105-108.
19. F. Leydier, C. Chizallet, A. Chaumonnot, M. Digne, E. Soyer, A.-A. Quoineaud, D. Costa and P. Raybaud, *J. Catal.*, 2011, **284**, 215-229.
20. F. Leydier, C. Chizallet, D. Costa and P. Raybaud, *Chem. Commun.*, 2012, **48**, 4076-4078.
21. L. Regli, A. Zecchina, J. G. Vitillo, D. Cocina, G. Spoto, C. Lamberti, K. P. Lillerud, U. Olsbye and S. Bordiga, *Phys. Chem. Chem. Phys.*, 2005, **7**, 3197-3203.
22. K. Chakarova and K. Hadjiivanov, *J. Phys. Chem. C*, 2011, **115**, 4806-4817.
23. P. Ugliengo, E. Garrone, A. M. Ferrari, A. Zecchina and C. Otero Areán, *J. Phys. Chem. B*, 1999, **103**, 4839-4846.
24. L. Mino, G. Spoto, S. Bordiga and A. Zecchina, *J. Phys. Chem. C*, 2012, **116**, 17008-17018.
25. A. Zecchina, S. Bordiga, G. Spoto, D. Scarano, G. Spanò and F. Geobaldo, *J. Chem. Soc., Faraday Trans.*, 1996, **92**, 4863-4875.
26. A. G. Pelmenschikov, G. Morosi, A. Gamba, A. Zecchina, S. Bordiga and E. A. Paukshtis, *J. Phys. Chem.*, 1993, **97**, 11979-11986.
27. G. Spoto, S. Bordiga, G. Ricchiardi, D. Scarano, A. Zecchina and E. Borello, *J. Chem. Soc., Faraday Trans.*, 1994, **90**, 2827-2835.
28. T. Shimanouchi, *Tables of molecular vibrational frequencies Consolidated Volume I*, National Bureau of Standards, Washington, 1972.
29. R. Buzzoni, S. Bordiga, G. Ricchiardi, C. Lamberti, A. Zecchina and G. Bellussi, *Langmuir*, 1996, **12**, 930-940.
30. F. Thibault-Starzyk, A. Vimont and J.-P. Gilson, *Catal. Today*, 2001, **70**, 227-241.